****

CHAPTER – II

PREPARATION & CHARACTERIZATION OF FERRITE

****

SECTION - A

PREPARATION OF FERRITES

2. Introduction

Modern ferrite materials are used in wide variety of applications. The usefulness of ferrites is determined by their physico-chemical properties which fall into two categories, intrinsic and extrinsic. Saturation magnetization, anisotropy, magnetostriction and Curie temperature are considered to be intrinsic properties, whereas, hysteresis, resistivity are supposed to be extrinsic properties. Extrinsic properties depend on structural aspects like grain size, porosity and impurities.

Polycrystalline ferrites are usually formed by solid state reaction between the component oxides. For the preparation of ferrites various methods are used. The most widely accepted method is the ceramic method. It makes possible the preparation of complex chemical compositions, desired microstructure and shape of final products. It is much more economical than the other methods. The grain growth, densification and microstructural features develop during sintering process. Ceramics have sufficient mechanical strength to allow it to be formed in desired shape. Ceramics provide away of avoiding undesired effects such as eddy current losses which can be suppressed by internal lamination along the grain boundaries [1].

2.A.1 Methods of ferrite preparation

Ferrites are prepared for the use of magnetic devices, either in polycrystalline or single crystal form. Different technique have been developed for the preparation of ferrites. In the preparation of ferrites, the starting materials are allowed to undergo solid state reaction. In the preparation of polycrystalline ferrite materials, basically four steps are involved.

1. Preparation of materials to form an intimate mixture in the desired composition.
2. Presintering and calcination
3. Converting the presintered material into fine powder and pressing the powder into required shape.
4. Final sintering to form the end product. Out of the different methods of preparation of ferrites, only the ceramic method is dealt with in greater details here.

Ceramic method

This is the most extensively used method for the commercial production of ferrites. High purity oxides are mixed together in desired proportions required for the final product. They are mixed manually or wet milled with steel balls for few hours. After milling, the mixture is dried up and sieved. The mixture is

calcined at elevated temperature and powdered. The powder is then pressed into a suitable shape with the help of hydraulic press and finally sintered. The purity of oxides, particle size and shapes are important for desired applications [2]. They must also posses high reactivity so that on mixing and after calcination the homogeneous ferrite can be achieved. The flow chart of stages involved in preparation of ferrites by this method is shown in Fig. 2.A.1.

2.A.2 Sintering

Sintering is the heat treatment process by which a mass of compacted powder is transformed into a dense object. There are two stages of sintering presintering and final sintering.

2.A.2a Presintering

The purpose of presintering is to decompose higher oxides and carbonates which reduce the evolution of gas in the final sintering process. Secondly, it assists in homogenizing of the material and also to reduce the variations in the compositions of raw materials. Lastly, it is necessary to control the shrinkage of the material which occurs during final sintering. The raw materials partly react to form final product during presintering and the amount of reaction depends on the

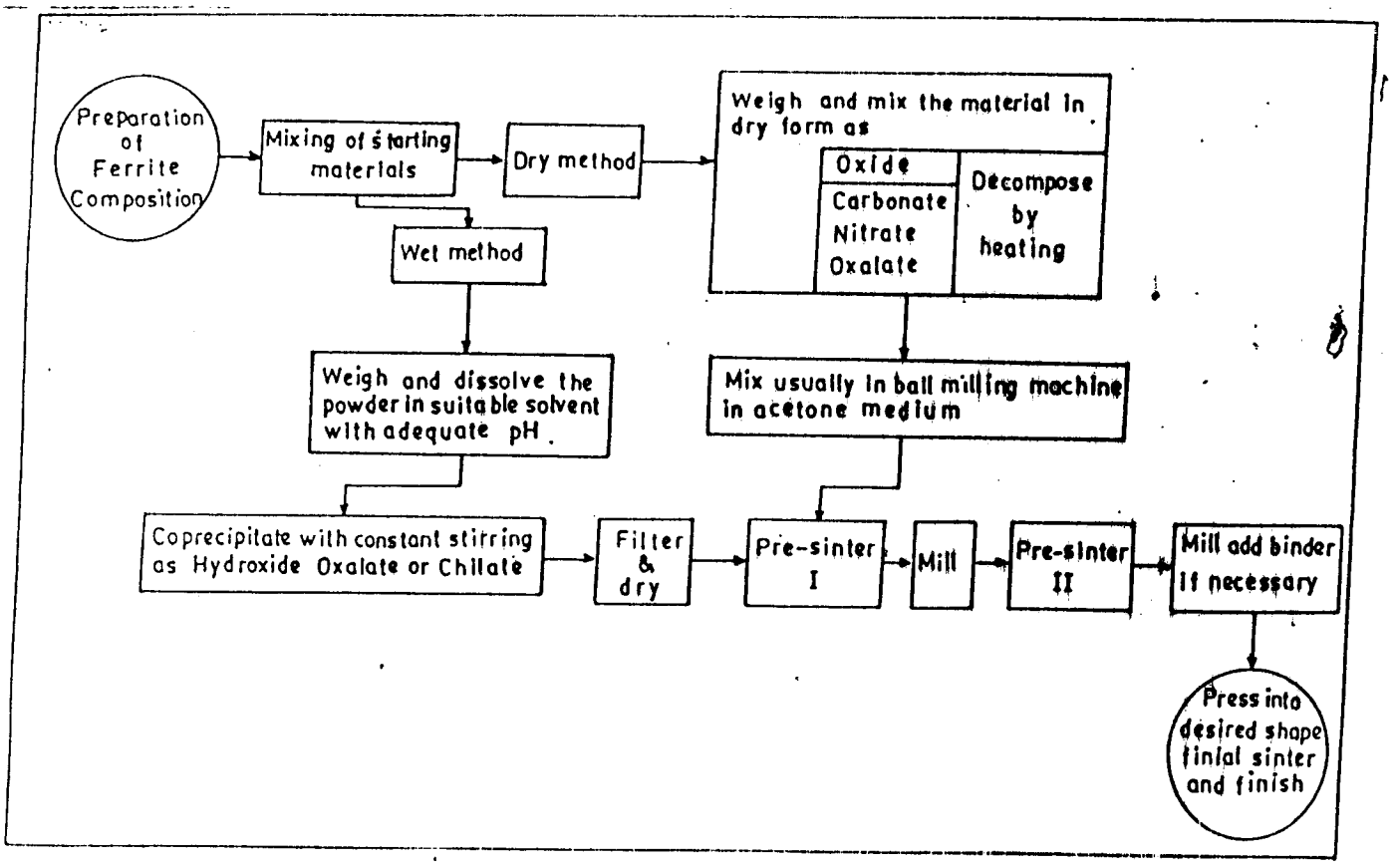

Fig. 2·A·1 – FLOW CHART OF STAGES INVOLVED IN PREPARATION OF FERRITES BY CERAMIC METHOD IN LAB.

reactivity of the components and on presintering temperature [3].

The ferrite is formed essentially in presintering but raw ferrite thus formed has poor qualities in two respects. First, its decomposition is not expected to be homogeneous and secondly, it contains pores as a result of the evolution of oxygen. Wagner [4] reports the use of high temperature furnace for presintering purpose.

2.A.2b Final sintering

For a good quality ferrite the grain size should be uniform. The pores should be intergranular and no discontinuous grain growth should occur. This can be achieved in the final sintering process. The sintering is done to increase the density. The control of grain size and pore distribution has been reviewed by many authors [5,6]. The microstructure mainly depends on the reactivity of the starting material and sintering temperature.

2.A.2c: Solid state reaction

The formation of the ferrite occurs by counter diffusion of cations through the oxygen lattice. This process is called as the solid state reaction mechanism.

The oxides to be used must be fine powders in order to be highly reactive. It is also recommended to have particles of the same size. The homogeneous mixture of metal oxide and ferric oxide (Fe_2O_3) is heated to a high temperature. The mechanism of diffusion takes place at this high temperature between M and Fe_2O_3. In the primary stage of the reaction, there exist only one phase boundary between the reactants. After the nucleation of the ferrite this initial phase boundary is replaced by two different phase boundaries, one between M and ferrite MFe_2O_4 and other between Fe_2O_3 and MFe_2O_4.

In this reaction stage, further progress takes place by the transport of reactants through the ferrite phase. The transfer mechanism to form MFe_2O_4 can be explained by three different models. According to Wagner [7], during the counter diffusion mechanism, only cations migrate in the opposite directions, the oxygen ions are being considered stationary.

According to second mode of transfer mechanism the anions take part in the diffusion process in which diffusion of single cation is compensated by an associated flux of anions instead of counter current of another cations. In the third mechanism, iron diffuse through the ferrite layer in the reduced state Fe^{2+}. During this, the oxygen is transported through the gas

phase, being given off at the MFe_2O_4/Fe_2O_3 interface and taken up again at the MO/MFe_2O_4 interface.

2.A.2d Hot pressing

The process of hot pressing has been increasingly used on an experimental scale during the last few years. Ferrites have been fabricated to very high density by hot pressing at low temperature. In this process, simultaneous applications of temperature and pressure takes place [8]. The powder is enclosed in a flexible container of rubber or plastic which may be evacuated and is compacted by immersing the container in an oil bath to which the pressure is applied.

The effect is to give much more uniformity and high density than the conventional methods. It also encourages continuous grain growth and favours to obtain low porosity and grain size. It seems apparent that pressure should lead to a high degree of compaction and enhance contact between grains during sintering. At 1000 °C ferrite grains have sufficient plasticity to flow to a considerable extent at high pressures. It is favourable to produce high density compacts in which the original grain size is maintained.

2.A.3 Actual method for preparation of ferrite sample

The standard ceramic technique involving double sintering was used to prepare Ni-Al ferrites with general formula $NiAl_xFe_{2-x}O_4$. Six samples with x = 0.0, 0.2, 0.4, 0.6, 0.8 and 1.0 were prepared. High purity oxides were mixed together in stoichometric proportions and mixed physically in agate mortar in acetone medium. The mixture was presintered at 900 °C for 8 hours in air medium. The fine powder of resultant ferrites were obtained.

The pellets were prepared by pressing the powder in a die of 1.5 cm diameter with the help of hydraulic press by applying the pressure of about 6 to 8 tones per square inch for about 5 to 10 minutes. The final sintering was carried out at 1150 °C for about 12 hours in air medium. The pellets were furnace cooled at the rate of 80 °C/hour. The physical densities were calculated with the help of weight and dimension data, whereas the x-ray densities were calculated from the crystallographic data.

SECTION - B

X-RAY DIFFRACTION STUDIES

2.B.1 Introduction and principles of X-ray diffraction

X-ray diffraction technique is a well established tool for the study of crystal structure of materials. The characterization of ferrites can be done by using

X-ray diffraction. X-ray diffraction method was developed by Bertaut [9], Warren and Aberbach [10]. This method is also applicable for the determination of crystalline size distribution of materials.

The spinel structure of $MgAl_2O_4$ was first confirmed by Bragg [11] using X-ray diffraction. Electron and neutron diffraction are also employed in determining the crystal structure of ferrites. The neutron diffraction study of ferrite is carried out by the number of workers [12-14]. In the present study X-ray diffraction is used to -

1. Confirm the completion of solid state reaction
2. Observe the impurity phases
3. Determine the lattice constant, interplaner distances, site radii and bond lengths etc.

Several workers [15 to 25] have characterized the ferrites by using X-ray and neutron diffraction[15 - 25].

Bragg's Law

A monochromatic X-ray beam incident on thousands of randomly oriented crystallites in powder form, gets reflected from the sets of atomic planes in accordance with the Bragg's law.

$$2d_{hkl} \text{ Sin } \theta_{hkl} = N \lambda \quad \ldots \quad 2.1$$

where, d_{hkl} - is the interplaner distance of crystal planes of Miller indices (hkl)

n - integer

θ - glancing angle

In most cases, the first order diffraction (n=1) is used and Bragg's law takes the form,

$$\lambda = 2d_{hkl} \sin \theta_{hkl} \quad \ldots \quad 2.2$$

It can be shown that for the cubic crystal

$$d_{hkl} = \frac{a}{(h^2+k^2+l^2)^{1/2}} \quad \ldots \quad 2.3$$

where, a = lattice constant

From eqn. (2.2) and (2.3) we get for lattice parameter.

$$a = \frac{\lambda}{2 \sin\theta} (h^2+k^2+l^2)^{1/2} \quad \ldots \quad 2.4$$

2.B.2 Experimental methods of X-ray diffraction

Diffraction by crystal is possible only when the Bragg's law is satisfied. This can be made possible by continuously varying either λ or θ during the experiment.

The way in which these quantities are varied gives rise to three important diffraction methods.

Method	λ	θ
Laue method	variable	fixed
Rotating crystal method	fixed	variable
Powder method	fixed	variable

Here, only the powder method is discussed briefly.

2.B.2a Powder method

The most economic and widely used technique to establish single phase formation of ferrites is the X-ray powder diffraction method.

X-ray diffractometer works on the principle of Bragg's law. When a monochromatic beam of X-ray radiations is incident on the thousands of randomly oriented crystallites, it gets reflected from the sets of atomic planes in accordance with the Bragg's law. The diffraction occurs simultaneously from the individual crystallites that happen to be oriented with planes having the same angle of incidence θ . Recently, the counter diffractometer have been developed and are commercially available to record the diffractograms. In counter diffractometer, the sample is placed at the center, so that X-rays falls on the plane surface of the sample. About the same axis, rotates an arms carrying a Geiger counter which records the diffracted X-rays. When the sample is rotated by the angle θ the counter is turned through 2θ . After complete scanning the XRD machine gives a record showing the variation of intensities of diffracted X-rays with angle θ. This method was first developed by Debye and Scherrer [26] and independently by Hull [27].

2.B.3 Experimental Techniques

X-ray diffraction pattern of the samples in the present case were recorded with the help of computerized XRD (λ = 1.5418 $\mathring{A}$) at USIC, Shivaji University, Kolhapur. The X-ray diffraction patterns were taken with 2θ values ranging between 20° to 80°.

For cubic crystal structure interplaner distance is given by, eqn. (2.3) as,

$$d_{hkl} = \frac{a}{(h^2+k^2+l^2)^{1/2}} \quad \ldots \quad 2.3$$

Using Bragg's law,

$$\lambda = \frac{2a \sin\theta}{(h^2+k^2+l^2)^{1/2}} \quad \ldots \quad 2.5$$

This equation can be used to determine type of crystal structure.

Equation (2.5) can be written as,

$$\frac{\sin^2\theta}{(h^2+k^2+l^2)} = \frac{\sin^2\theta}{S} = \frac{\lambda^2}{4a^2} \quad \ldots \quad 2.6$$

since the sum S = $(h^2+k^2+l^2)$ is always integral and $\lambda^2/4a^2$ is a constant for any one pattern. The problem of indexing the pattern of a cubic substance is one of finding a set of integers S which will yield a constant quotient when divided one by one, the observed $\sin^2\theta$ values. Once set of S are found using (2.5) (h,k,l) values can be found out.

With the help of standard spinel structure, it is possible to calculate lattice parameter for different planes of diffraction in diffractograms. The prominent line in the X-ray diffraction pattern of the spinel structure corresponds to (311) plane. By knowing the values of glancing angle (θ), it is possible to calculate value of lattice parameter 'a'. Usual procedure is followed to calculate lattice parameters, interplaner spacing 'd' and Miller indices (h,k,l).

For cubic samples, it is possible to calculate the radii of tetragonal (A) and octahedral (B) sites with the help of relation,

$$r_A = (U-1/4)\, a\sqrt{3} - R_o$$

and $$r_B = (5/8 - U)\, a - R_o \qquad \ldots \quad 2.7$$

and bond lengths in cubic crystal for A and B sites were calculated by equation,

$$R_A = a\sqrt{3}\,(\delta + 1/8)$$

and $$R_B = a\,(1/16 - \delta/2 + 3\delta^2)^{1/2} \qquad \ldots \quad 2.8$$

where, δ - deviation from oxygen parameter (U)

$$\delta = U - U_{ideal}$$

As $U = 0.381$ A° for Nickel ferrite [28] and

$U_{ideal} = 0.375$ A°

Ro = radius of oxygen ion = 1.35 A°.

The X-ray density (dx), physical density (da) and porosity of ferrite samples were calculated by using the relation as,

$$d_x = \frac{8M}{Na^3} \quad \ldots \quad 2.9$$

$$d_a = m/\pi r^2 t \quad \ldots \quad 2.10$$

$$\text{and porosity} = P\ (\%) = \frac{d_x - d_a}{d_x} \times 100 \quad \ldots \quad 2.11$$

where, M = molecular weight of sample

N = Avogadro's Number

a = lattice parameter

m = mass of pellet

r = radius of pellet

t = thickness of pellet.

2.B.4 Results and Discussion

The X-ray diffraction patterns for the samples in the system $NiAl_xFe_{2-x}O_4$ with x = 0.0, 0.2, 0.4, 0.6, 0.8 and 1.0 are shown in Figs. 2.B.1 to 2.B.6. The diffraction peaks indicate the f.c.c. cubic nature of the samples. The planes in the diffraction pattern of spinel structure are (220), (311), (400), (422), (333) and (440) etc.

The variation of lattice parameter with content of Al^{3+} is shown in Fig. 2.B.7. The Tables 2.B.1 - 2.B.6 contain data on observed and calculated d values and Miller indices of different planes. The lattice parameter (a), bond lengths (R_A,R_B) and site radii (r_A,r_B) are presented in Table 2.B.7.

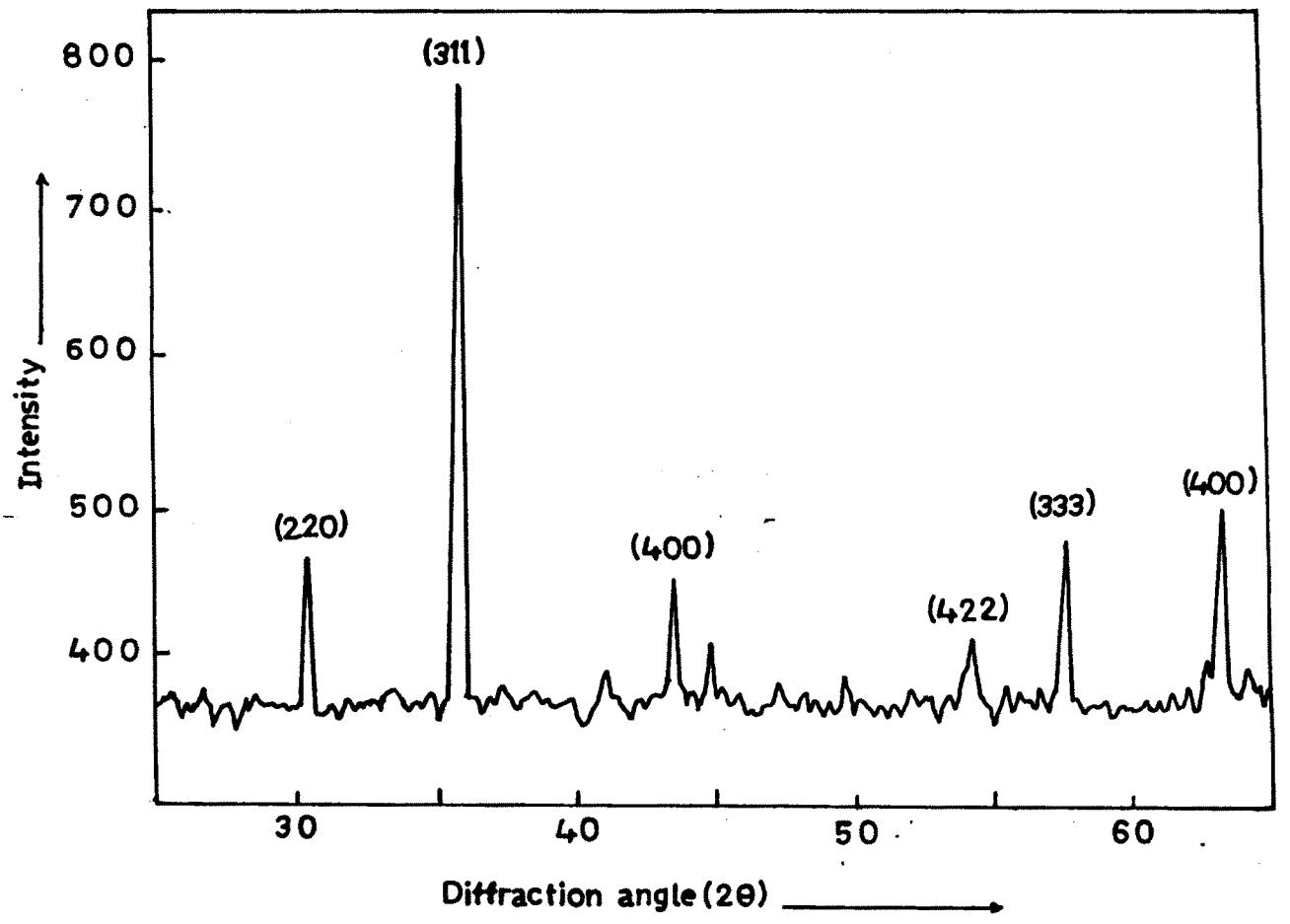

Fig.2.B.1. X-ray diffraction pattern of $NiFe_2O_4$.

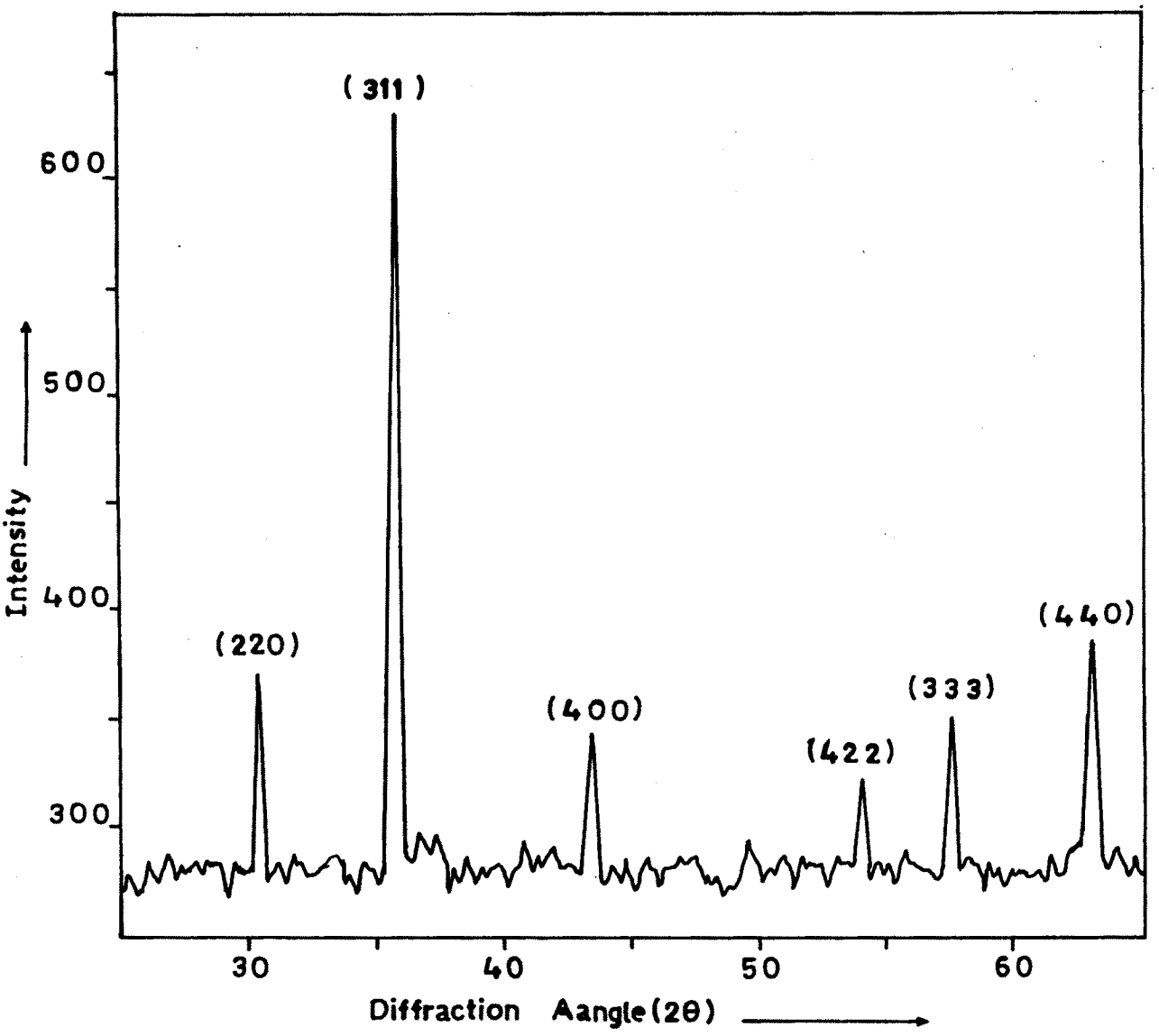

Fig.2.B.2. X ray diffraction pattern of $NiAl_{0.2}Fe_{1.8}O_4$

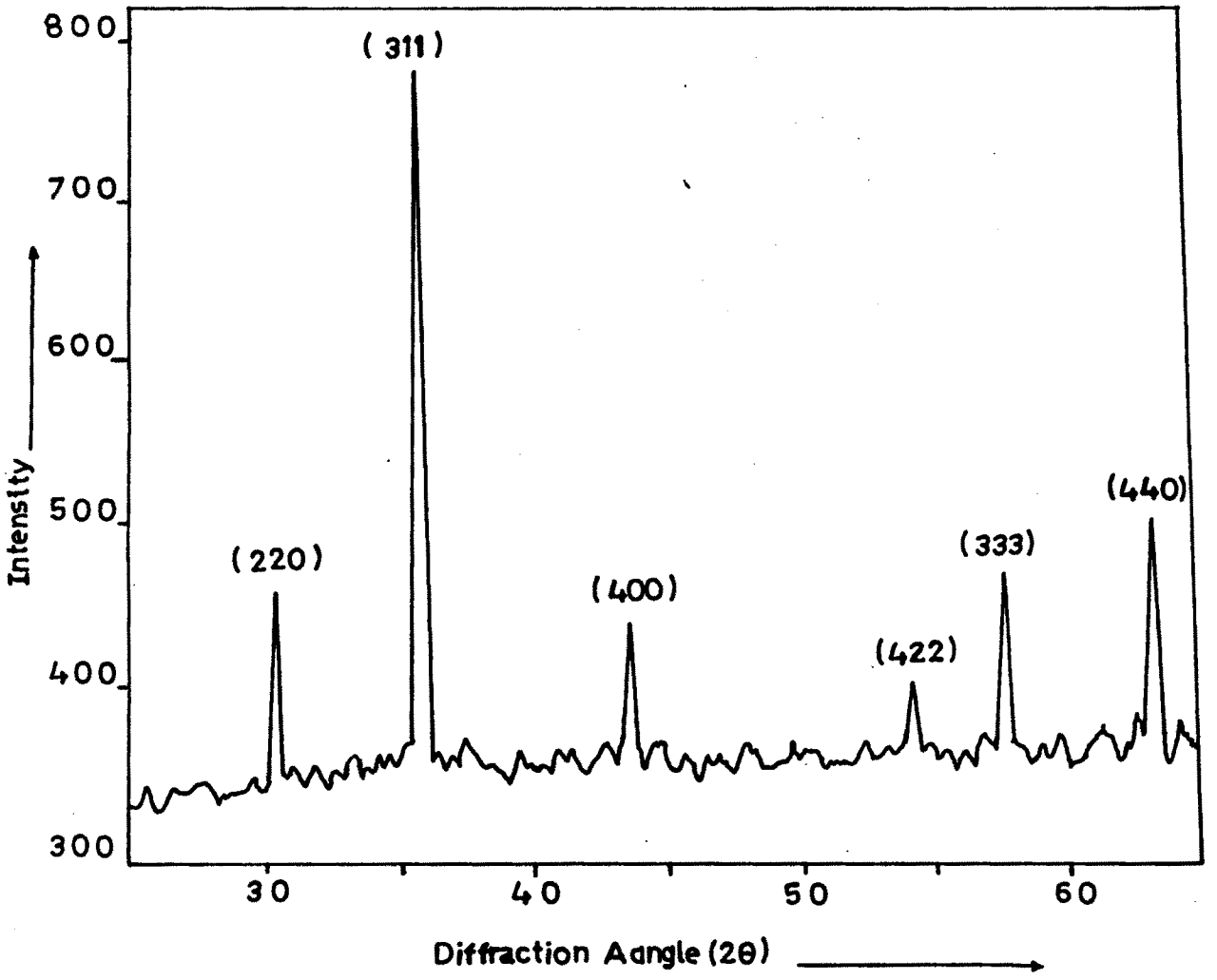

Fig.2.B.3.X-ray diffraction pattern of $NiAl_{0.4}Fe_{1.6}O_4$

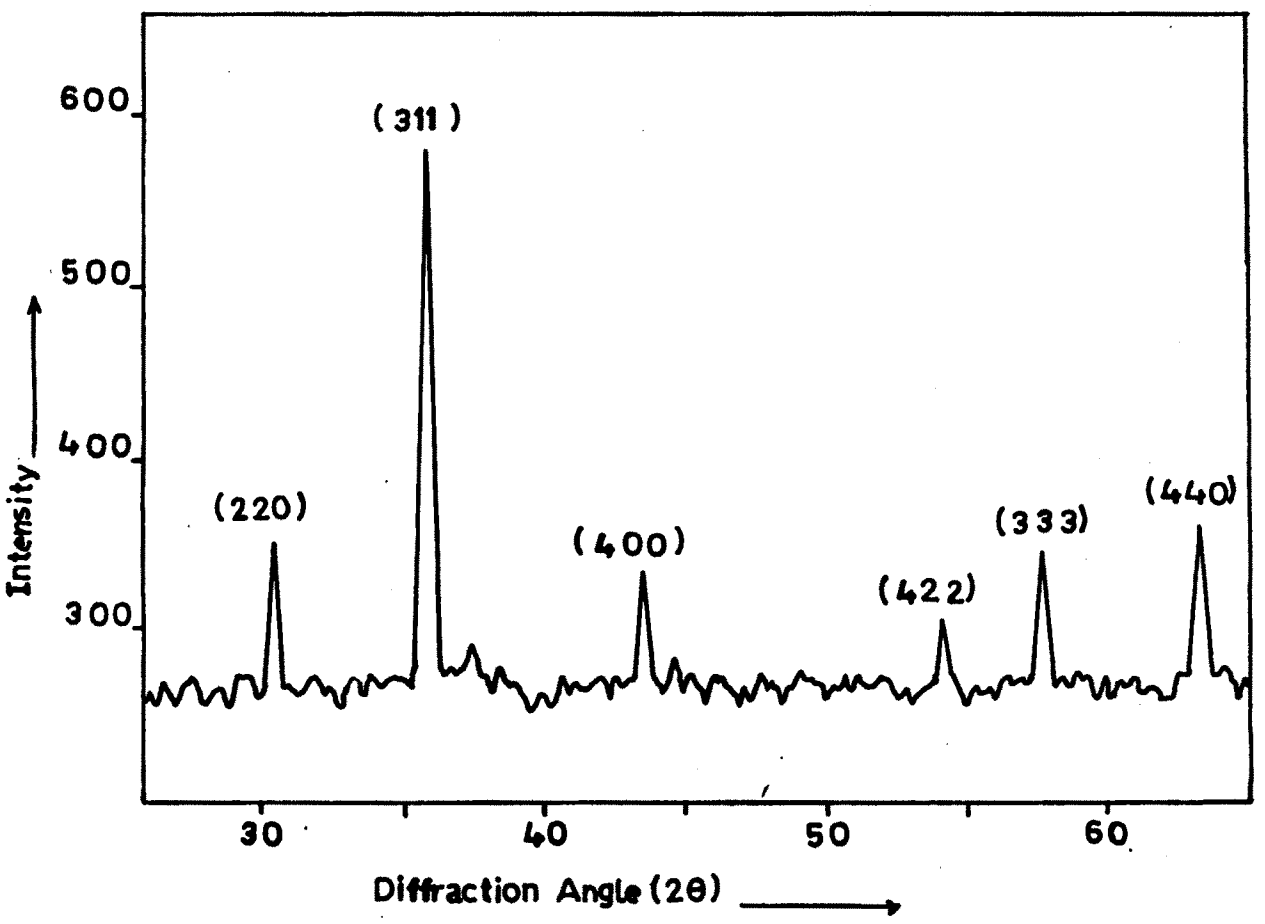

Fig. 2.B.4. X-ray diffraction pattern of $NiAl_{0.6}Fe_{1.4}O_4$

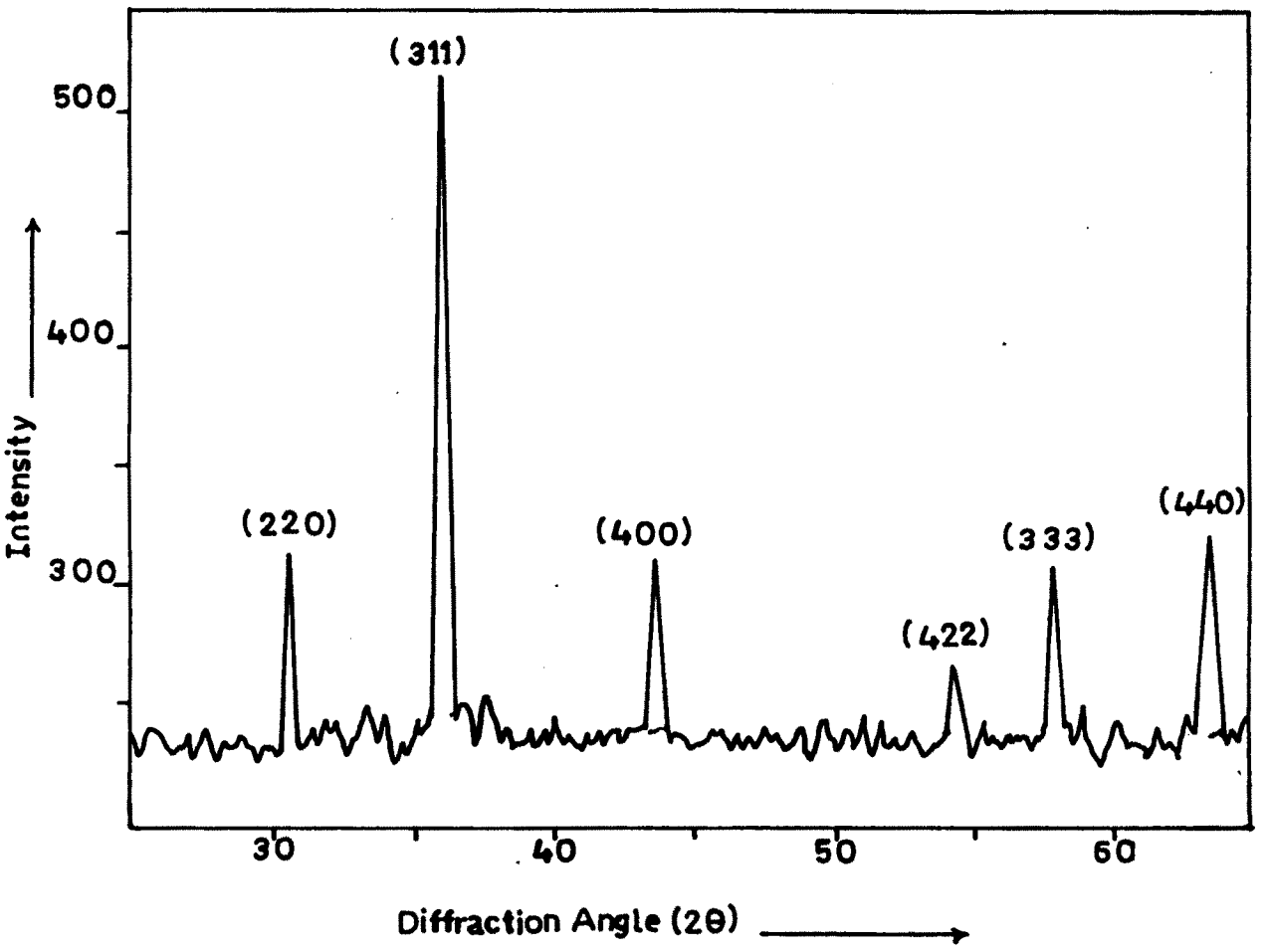

Fig.2.B.5. X-ray diffraction pattern of $NiAl_{0.8}Fe_{1.2}O_4$

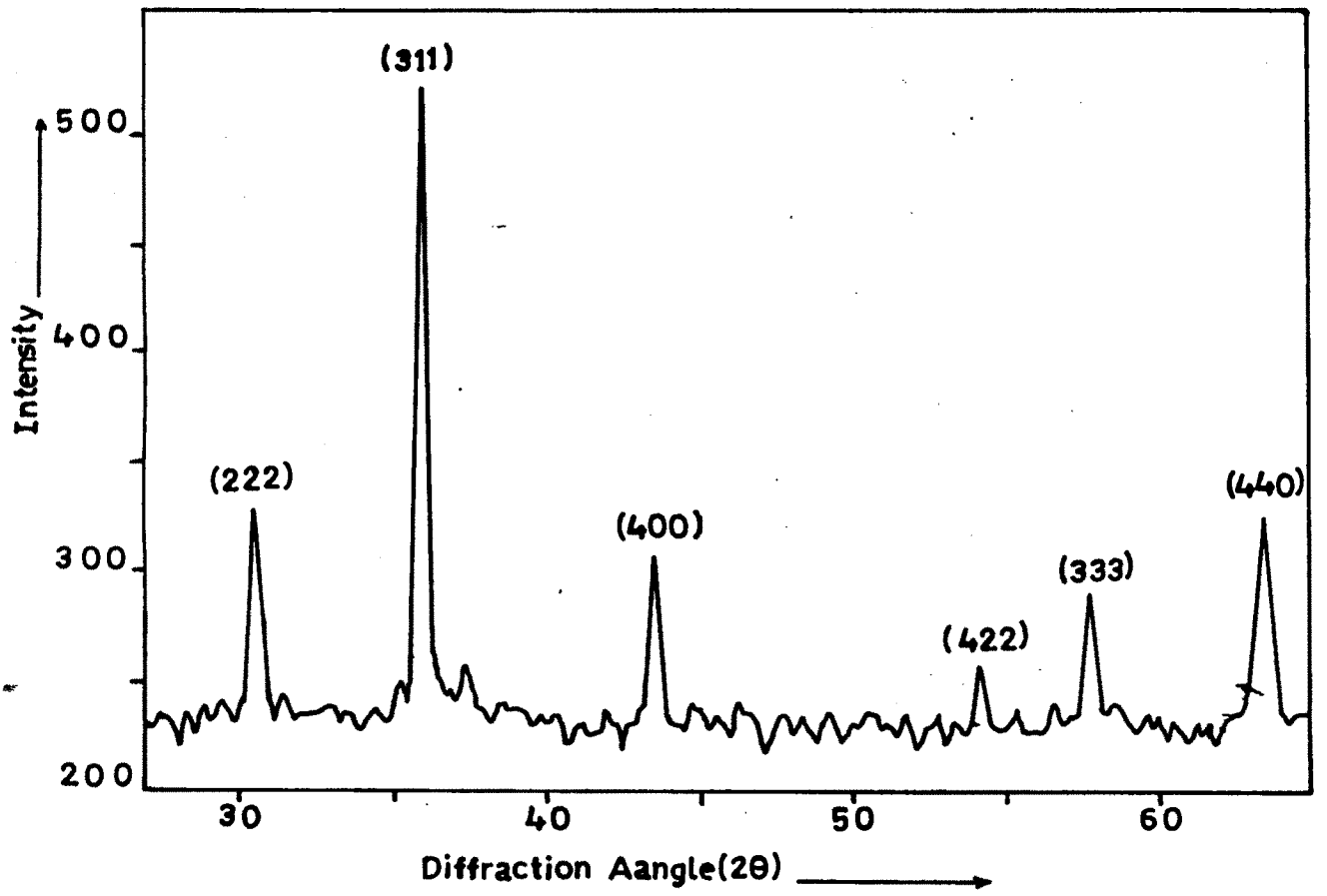

Fig.2.B.6. X-ray diffraction of $NiAlFe_2O_4$

TABLE - 2.B.1

X-ray diffraction data of $NiFe_2O_4$

Wavelength - 1.54249 Å, Structure - Cubic

Lattice parameter - 8.326 Å

Sr.No.	2θ (deg)	$d_{cal.}$ (Å)	d_{obs} (Å)	d_{mean} (Å)	(h k l)
1.	30.280	2.9476	2.9493	2.9495	2 2 0
2.	35.690	2.5134	2.5137	2.5136	3 1 1
3.	43.390	2.0842	2.0838	2.0840	4 0 0
4.	54.145	1.7019	1.6925	1.6970	4 2 2
5.	57.375	1.6045	1.6047	1.6046	3 3 3
6.	63.030	1.4738	1.4736	1.4737	4 4 0

TABLE - 2.B.2

X-ray diffraction data of $NiAl_{0.2}Fe_{1.8}O_4$

Wavelength - 1.54249 Å, Structure - Cubic

Lattice parameter - 8.332 Å

Sr.No.	2θ (deg)	$d_{cal.}$ (Å)	d_{obs} (Å)	d_{mean} (Å)	(h k l)
1.	30.300	2.9476	2.9474	2.9475	2 2 0
2.	35.690	2.5137	2.5137	2.5137	3 1 1
3.	43.430	2.0843	2.0819	2.0830	4 0 0
4.	54.000	1.7018	1.6925	1.6992	4 2 2
5.	57.455	1.6045	1.6026	1.6035	3 3 3
6.	63.115	1.4738	1.4719	1.4728	4 4 0

TABLE - 2.B.3

X-ray diffraction data of $NiAl_{0.4}Fe_{1.6}O_4$

Wavelength - 1.54249 Å, Structure - Cubic

Lattice parameter - 8.326 Å

Sr.No.	2θ (deg)	$d_{obs.}$ (Å)	d_{obs} (Å)	d_{mean} (Å)	(h, k, l)
1.	30.325	2.9430	2.9451	2.9440	2 2 0
2.	35.745	2.5098	2.5099	2.5098	3 1 1
3.	43.430	2.0810	2.0819	2.0815	4 0 0
4.	54.020	1.6991	1.6962	1.6977	4 2 2
5.	57.450	1.6020	1.6028	1.624	3 3 3
6.	63.070	1.4715	1.4728	1.4721	4 4 0

TABLE - 2.B.4

X-ray diffraction data of $NiAl_{0.4}Fe_{1.4}O_4$

Wavelength - 1.54249 Å, Structure - Cubic

Lattice parameter - 8.311 Å

Sr.No.	2θ (deg)	$d_{cal.}$ (Å)	d_{obs} (Å)	d_{mean} (Å)	(h k l)
1.	30.375	2.9391	2.9403	2.9397	2 2 0
2.	35.795	2.5065	2.5065	2.5065	3 1 1
3.	43.505	2.0783	2.0785	2.0784	4 0 0
4.	54.070	1.6969	1.6947	1.6958	4 2 2
5.	57.605	1.5998	1.5988	1.5993	3 3 3
6.	63.385	1.4695	1.4662	1.4678	4 4 0

TABLE - 2.B.5

X-ray diffraction data of $NiAl_{0.8}Fe_{1.2}O_4$

Wavelength - 1.54249 Å, Structure - Cubic

Lattice parameter - 8.308 Å

Sr.No.	2θ (deg)	$d_{cal.}$ (Å)	d_{obs} (Å)	d_{mean} (Å)	(h k l)
1.	30.525	2.9317	2.9262	2.9260	2 2 0
2.	35.890	2.5001	2.5001	2.5001	3 1 1
3.	43.490	2.0730	2.0792	2.0761	4 0 0
4.	54.260	1.6925	1.6892	1.6909	4 2 2
5.	57.610	1.5958	1.5987	1.5973	3 3 3
6.	63.430	1.4658	1.4653	1.4656	4 4 0

TABLE - 2.B.6

X-ray diffraction data of $NiAlFe_2O_4$

Wavelength - 1.54249 $\AA$, Structure - Cubic

Lattice parameter - 8.300 $\AA$

Sr.No.	2θ (deg)	$d_{cal.}$ ($\AA$)	d_{obs} ($\AA$)	d_{mean} ($\AA$)	(h k l)
1.	30.385	2.9380	2.9394	2.9387	2 2 0
2.	35.810	2.5055	2.5055	2.5055	3 1 1
3.	43.490	2.0795	2.0792	2.0794	4 0 0
4.	54.020	1.6963	1.6962	1.6963	4 2 2
5.	57.610	1.5993	1.5987	1.5990	3 3 3
6.	63.285	1.4690	1.4683	1.4687	4 4 0

It is clear from the Tables 2.B.1 to 2.B.6 that the observed and calculated d values are in good agreement with each other for all the indexed planes.

As seen from Fig. 2.B.7 the value of lattice parameter goes on decreasing with increasing Al^{3+} content. The solubility of IIIB group metal such as Al, Ga and B in Nickel ferrite clearly shows a decrease in lattice constant with increasing amount of these additives [32]. Since the ionic radius of Al^{3+} (0.57 A^{o}) is smaller as compared to that of Ni (0.78 A^{o}) and Fe^{3+} (0.67 A^{o}) the lattice parameter is expected to decrease. Similar result is observed in Al substituted Ni-Zn ferrite by Kakatkar [33]. Al^{3+} ion have a strong site preference for B-site. The partial replacement of Fe^{3+} by Al^{3+} on the octahedral site causes the shrinkage of unit cell.

In the present work, the value of lattice parameter for Nickel ferrite is 8.337 A^{o} which agrees fairly well with earlier reported values viz. 8.335 A^{o} [29] and 8.339 [30,31].

The values of bond length and site radii calculated using the relations (2.7) and (2.8) are presented in Table 2.B.7. The value of oxygen parameter used in the present calculationis 0.381 $\mathring{A}$. The variation of bond length (R_A and R_B) and site radii (rA and rB) with content of Al is shown in Fig. 2.B.8 and

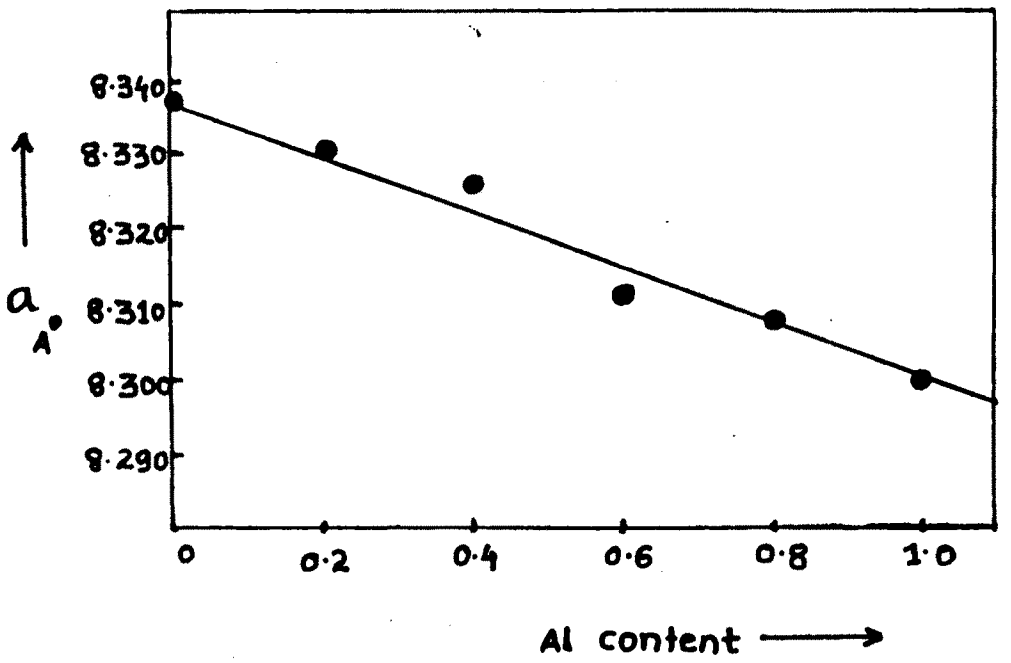

FIG. 2·B·7 VARIATION OF LATTICE PARAMETER (a) AS A FUNCTION OF Al CONTENT.

TABLE - 2.B.7.

Data on lattice parameter, bond lengths (R_A, R_B) and site radii (r_A, r_B) for NiAlxFe2-xO4

X	Lattice Parameter(A)	R_A A°	R_B A°	r_A A°	r_B A°
0.0	8.337	1.8917	2.0318	0.542	0.684
0.2	8.326	1.8892	2.0291	0.539	0.681
0.4	8.332	1.8905	2.0305	0.540	0.683
0.6	8.311	1.8858	2.0254	0.536	0.678
0.8	8.308	1.8851	2.0247	0.535	0.677
1.0	8.300	1.8833	2.0228	0.533	0.675

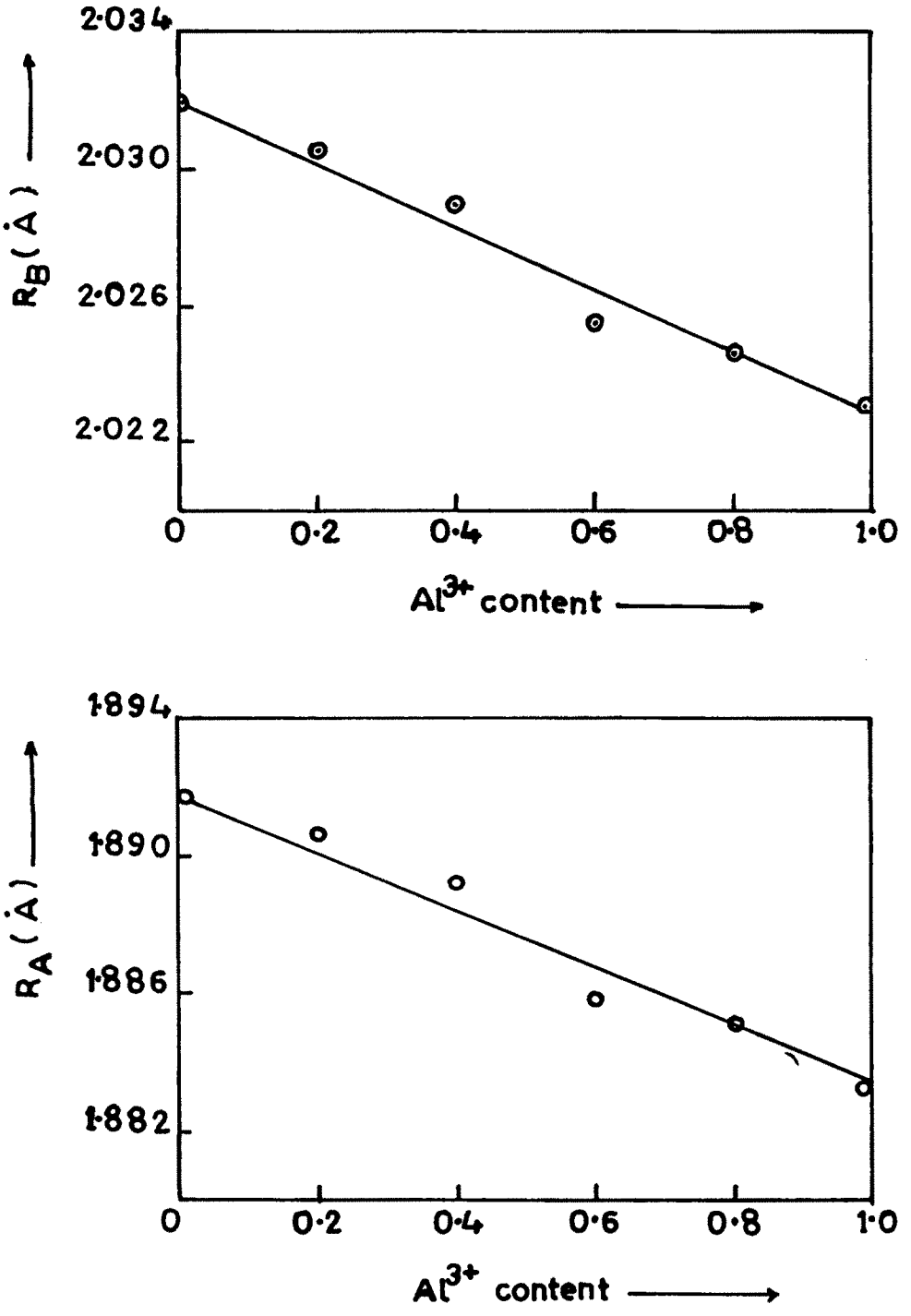

Fig.2.B.8. Variation of bond length (R_A, R_B) as a function of Al content.

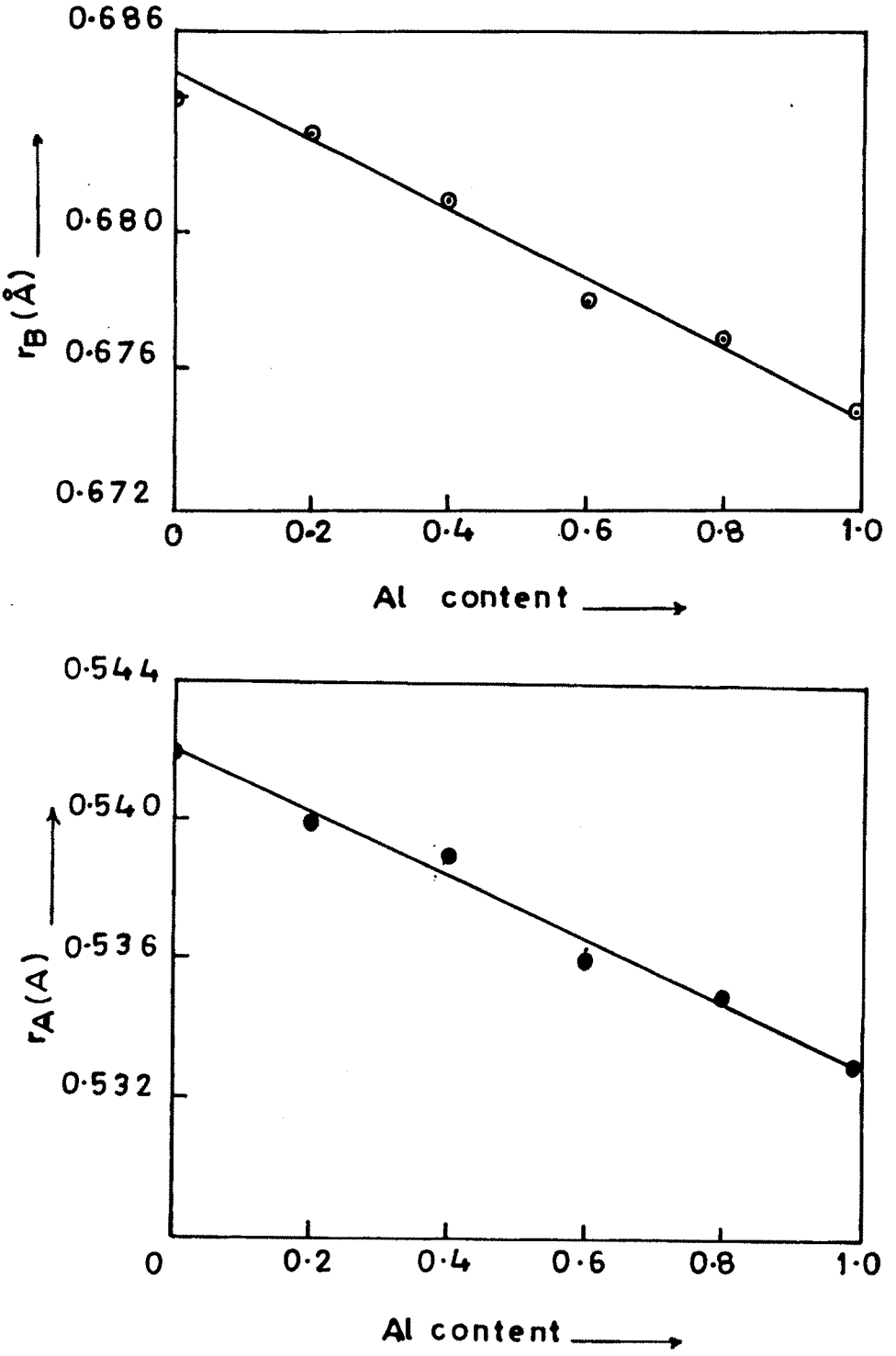

FIG.2.B.9. VARIATION OF SITE RADII (r_A, r_B) AS A FUNCTION OF Al CONTENT.

TABLE - 2.B.8

X-ray density, actual density and porosity data for

NiAlxFe2-xO4

x	dx-ray 'dx' gm / cc	dactual'da' gm / cc	Porosity ' % ' (p)
0.0	5.3731	3.220	34.45
0.2	5.2482	3.3796	35.60
0.4	5.1269	3.0401	40.70
0.6	5.0229	2.9137	41.99
0.8	4.8952	3.0046	38.62
1.0	4.7746	3.1483	34.062

2.B.9. It is clear that bond length and site radii decrease with increasing Al content.

The bond length R_B is always greater than Ra. Similar results are in Al substituted Ni-Zn ferrite (33).

Data on x-ray density, actual density and porosity is given in Table 2.B.8. The porosity of the samples is of the order of 30 to 40%.

SECTION - C

INFRA-RED STUDIES

2.C.1 Introduction

Studies of spectral relationships between structure and electromagnetic radiation of ferromagnetic materials are useful in understanding their properties. The properties of these materials depend on the precise configuration of atoms or ions in their structure. Methods of non-destructive analysis such as IR of wavelength 1 μ to 1mm are specially suitable to determine such a configuration. In particular the vibrational, electronic and magnetic dipole spectra can give information of about the position and valency of the ions in the crystal lattice. The IR spectroscopy can be used to -

1. Study of cation distribution
2. Study of deformation of cubic spinel structure

3. Determine co-ordination of cations in the structure

4. Detect the presence of absorption bands in ferrites.

The spectra which show two absorption bands between 200 cm^{-1} to 1000 cm^{-1}, is a common feature of all ferrites [34]. Absorption in this region is not restricted to this class of compounds but also occurs in many metallic oxides [35,36]. The bands arise from lattice vibrations of the oxygen ions against the cations. At higher frequencies, gradually increasing absorption caused by electronic transition is observed. According to Waldron [34], high frequency band (ν_1) is at 600 cm^{-1} is due to tetrahedral complexes and low frequency band (ν_2) at 400 cm^{-1}, is due to octahedral complexes.

Hafner [37], Tarte [38] and others [39,40] have applied IR spectroscopy to study the absorption bands in many normal as well as inverse spinel ferrites.

In ferrites two types of spectra are observed:

1. Electronic spectra due to electronic transitions
2. Vibrational spectra due to cation vibrations.

In case of ferrites the frequency of vibration depends upon the cation mass, cation oxygen bonding force and unit cell parameters.

2.C.2 Experimental Techniques

The IR spectra of sample were recorded on Perkin Elmer 783 IR spectrometer. The pellets used for recording spectra were prepared by mixing small amount of ferrite powder in KBr. The IR spectra in the frequency range 200-800 cm^{-1} were recorded at room temperature at USIC, Shivaji University, Kolhapur.

2.C.3 Results and Discussion

IR spectra of present samples are shown in Fig. 2.C.1 and 2.C.2. The spectra of all ferrite samples are used to locate the band positions which are noted in Table 2.C.1.

It has been pointed out earlier that vibrational frequencies depends on the mass of cations, cation oxygen bonding force, and unit cell dimensions [41]. Brabers [42] has classified the lattice vibrations of cubic spinels. According to this classification there are four IR active modes which are triply degenerate for the normal spinel. For inverse spinel and partially inverse spinels triply degenerate vibrations may split up into three vibrations. If the splitting is not too large and there is certain statistical distribution of various cations over the tetrahedral and octahedral sites, one cannot observe the splitting but only broadening of the absorption band.

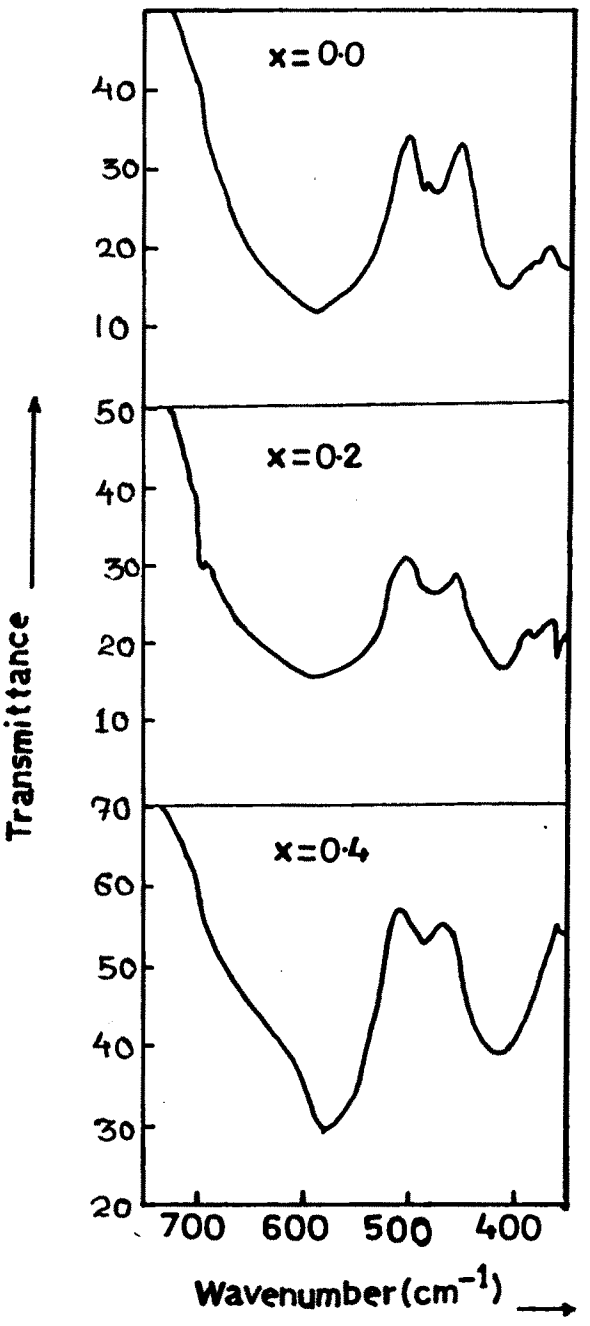

Fig.2.C.1. Infrared spectra of $NiAl_xFe_{2-x}O_4$ ferrites.

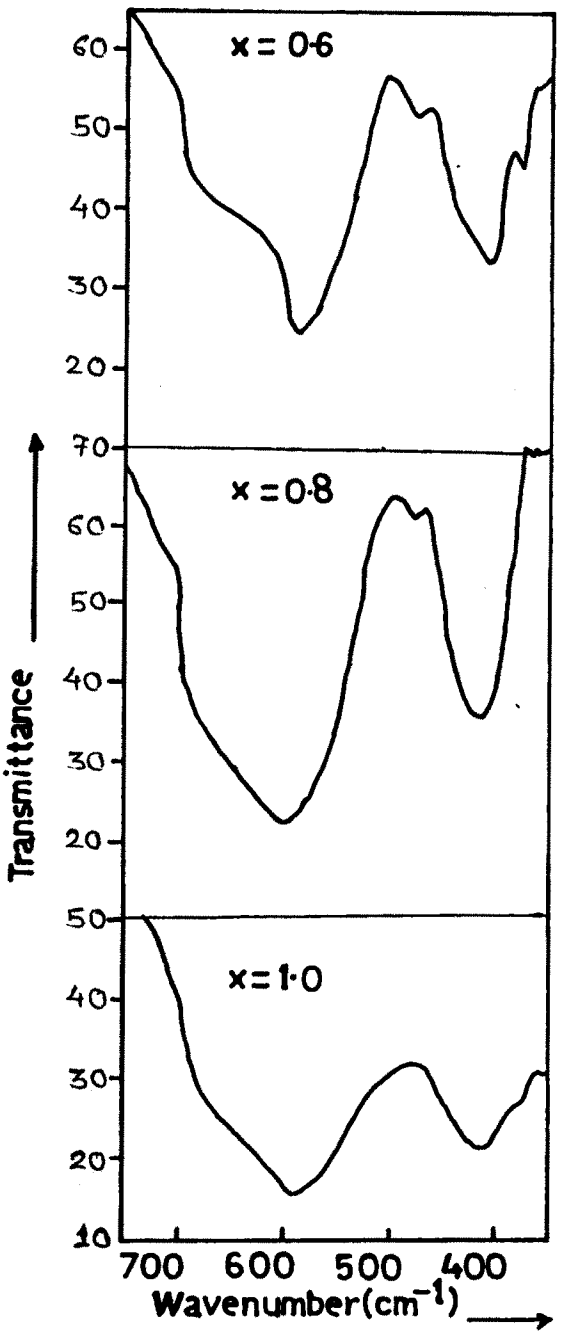

Fig.2.C.2. IR Spectra of $NiAl_xFe_{2-x}O_4$ ferrites.

TABLE - 2.C.1.

Lattice vibration frequencies for $NiAl_xFe_{2-x}O_4$

X	V_1 cm^{-1}	V_2 cm^{-1}	V_3 cm^{-1}
0.00	590	410	480
0.20	590	410	480
0.40	580	410	480
0.60	590	410	480
0.80	600	410	480
1.00	595	410	-

Klerk et. al. [42] have observed the third fundamental active mode of vibration in case of $MnFe_2O_4$. Recently Badrinath [43] has observed ν_3 band around 370 cm^{-1} by introducing Al^{3+} into lattice of $MnFe_2O_4$. The increase in intensity with increasing concentration of Al^{3+} is also observed by him.

The IR spectra of the present samples shown in Figs. 2.C.1 and 2.C.2 indicates that the high frequency band is in the range 580 cm^{-1} to 600 cm^{-1} and lower frequency band in the region 410 cm^{-1}. This difference in band position is expected because of difference in $Fe^{3+} - O^{2-}$ distance for octahedral and tetrahedral sites. Waldron [34] has studied IR spectra of number of ferrites and has observed two broad bands ν_1 and ν_2 at about 600 cm^{-1} and 400 cm^{-1} respectively due to tetrahedral and octahedral complexes. Many other workers [38,41,44,45] have observed the IR spectra in ferrites and they were same as that of Waldron.

An examination of the present IR spectra shows an additional peak around 480 cm^{-1}. The appearance of ν_3 band in IR spectra of ferrites is generally due to the divalent metal ion oxygen complexes in the octahedral sites [46].

The presence of Fe^{2+} ion causes the splitting of absorption due to local lattice deformation caused by Jahn-Teller effect leading to non-cubic component in the potential of crystal field.

In the present case, the samples with x = 0 to 0.8 show the splitting of octahedral band into new band ν_3. The intensity of ν_3 band goes on decreasing upto x = 0.8 and vanishes completely at x = 1.

References

1. Hirota E.
   J. Appli. Phys. Japan 5 (1966) 1125

2. Magee J.H., Morton V., Fisher R.D. and Lowe I.J.
   Ferrites, Proc. Int. Conf. Japan (1970) 217

3. Swallow D. and Jordon A.K.
   Proc. Brit. Ceram. Soc. 2 (1964) 1

4. Wagner U.
   J. Mag. Mag. Material 19 (1980) 99

5. Chol G., Damay F., Anuradon J.P. and Strivens M.P.
   'Electrical Communications', 43 (1968) 263

6. Stuijts A.L.
   Ferrites, Proc. Int. Conf. Japan 108 (1970)

7. Wagner C.
   Z. Phys. Chem. B-34 (1936) 309

8. Murvay P., Livey D.T. and Williams J.
   'Ceramic Fabrication process', W.D. Kingley (Edi.)
   Wiley, New York (1958) 147

9. Bertaut M.F.
   Compt. Rend. 228 (1949) 492

10. Warren B.E. and Aberbach B.L.
    J. Appli. Phys. 21 (1950) 595

11. Bragg W.L.
    Nature (London) 95 (1915) 516

12. Shull C.G., Wollan E.O. and Kochlar W.C.
    Phys. Rev. 84 (1952) 912

13. Hastings J.M. and Corliss L.M.
    Rev. Mod. Phys. 25 (1953) 114

14. Prince E. and Treuting R.G.
    Acta. Cryst. 9 (1956) 1025

15. Srivastava C.M., Srinivasan G. and Nandikar N.G.
    Phys. Rev. 19 (1979) 499-507

16. Jadhav S.P., Patil B.L. and Sawant S.R.
    IJP 63 A (1989), 818-820

17. Patil B.L., Sawant S.R., Patil S.A. and Patil R.N.
    Czech. J. Phys. 43, 2, (1993) 179-185

18. Patil S.A., Otari S.M., Patil M.G., Patil A.B., Soudagar M.K., Patil B.R. and Sawant S.R.
Solid State Communication 78, 1, (1991) 39-42

19. Radhakrishna N., Parajape S.K., Murthy M.R., Begum R.J., Madhav Rao L. and Satyamurthy N.S.
Solid State Phys. Symp. Bombay, India 3 (1972) 645

20. Patil R.S., Suryawanshi S.S., Kakathar S.V., Sankpal A.M., Ghodake V.R., Patil S.A. and Sawant S.R.
Bull. Mater. Sci. 17,2 (1994), 111-119

21. Satyamurthy N.S., Natera M.G., Begum R.J. and Youssef S.I.
Phys. Rev. 181 (1969) 181

22. Satyamurthy N.S., Natera M.G., Begum R.J. and Youssef S.I.
Proc. of ICF Japan (1970)

23. Bhise B.V., Dongare M.B., Patil S.A. and Sawant S.R.
J. Mat. Sci. Lett. 10 (1991) 922-924

24. Newnham R.E., Sankar S.G. and Patil K.C.
J. Appli. Phys. 63, 8 (1988) 3789-3791

25. Prakash C. and Baijal J.S.
J. Less Common Met. 107 (1985) 51-57

26. Debye P. and Scherrier P.
Physics 17 (1916) 277 and 18 (1977) 219

27. Hull A.N.
Phy. Rev. 9 (1916) 564 and 10 (1917) 661

28. Standley K.J.
"Oxide Magnetic Materials",
Oxford Univ. Press London (1962) 64

29. Wilson D.F. and Douglas D.L.
Material Science Monograph IS, Transport in Non-stoichiometric compounds.
Proc. of First Int. Conf. Aug. 27-30 (1980)

30. Kachi S., Momiyama K. and Shimizu S.
J. Phys. Soc. Japan 18 (1963) 106

31. Takai T. and Chiba S.
J. Phys. Soc. Japan 21 (1966) 1255

32. Tasaki J. and Izushi T.
Govt. Indu. Research Institute Nagoya, Japan
Colloque C1, Supplement au A° 4, Tome 38, Av
(1977) C1 175

33. Kakathar S.V.
Ph.D. Thesis, Shivaji University, Kolhapur (1993)

34. Waldron R.D.
Phys. Rev. 99, 16, 1727 (1955)

35. Harrier L.
J. Opt. Soc. Amer 45, 27, (1955)

36. Matossi F.
J. Chem. Phys. 19 (1951) 1543

37. Hafner S.T.
Z. Krist, 115 (1961) 331

38. Tarte P.
Spectrochim Acta. 19 (1963) 49

39. Preudhomme J.
Spectrochim Acta 26 A (1970) 985

40. White R.B. and De-Angelish B.A.
Spectrochim Acta 23 A (1963) 985

41. Murthy V.R.K., Reddy K.V., Chitrasankar S. and
Sobhanadri J.
Indian J. Pure and applied Phys. 36 (1978) 79

42. Klerk J. and Brabers V.A.M.
Solid State Communication 14 (1974) 613

43. Badrinath K.V.S.
Phys. Stat. sol. (a) 91 (1985) 19

44. Pakhomova N.L. and Christopher V.
Phys. Stat. Solidi (a) 105, (1987) 543

45. Reddy P.V. and Salagram M.
Physica Status Solidi (a) 100 (1987) 639

46. Patil S.H.
Ph.D. Thesis Shivaji University, Kolhapur (1993)